Turbulent mixing of a passive scalar in the ocean mixed layer

Neeraja Bhamidipati[a,*], Andre N. Souza[b], Glenn R. Flierl[b]

[a] *BP Institute for Multiphase Flow, Department of Earth Sciences, University of Cambridge, Madingley Rise, Cambridge, CB3 0EZ, United Kingdom*
[b] *Department of Earth, Atmospheric and Planetary Sciences, Massachusetts Institute of Technology, 77 Massachusetts Ave, Cambridge, MA 02139, United States*

Abstract

We study the 2D turbulent mixing of a passive scalar in the ocean mixed layer. As an example, we examine a steady-state convective mixed layer in which the boundary conditions are chosen so that the system reaches a dynamical equilibrium. In this idealized case, we parameterize the horizontally and temporally averaged fluxes as a functional of the horizontally and temporally averaged property gradients. Here, $\langle w'c' \rangle = -\int \mathrm{d}z' \mathcal{K}(z|z') \partial \langle c \rangle / \partial z'$, where $\mathcal{K}(z|z')$ is the eddy diffusivity kernel which describes the vertical transport by eddies at any vertical location z. The full kernel $\mathcal{K}(z|z')$ is computed by adding passive scalars to a buoyancy-driven flow field in a 2D DNS of the ocean surface layer. This functional form of the eddy diffusivity highlights both local and non-local effects of the mixing of a passive scalar, and is based on an unapproximated representation of the idealized physics. This type of formulation can be further extended to other problems in turbulence concerning the mixing of a passive scalar to determine a parameterization based on an accurate representation of ocean physics.

Keywords: Mixed layer, eddy flux, turbulence, parameterization

1. Introduction

The ocean mixed layer mediates the exchange of mass, momentum and energy between the ocean and the atmosphere (Kantha and Clayson, 1994). The depth of these layers can range from tens to thousands of meters and exhibits large seasonal variations depending on the latitude. The mixing within the surface layer is driven by a range of factors. In the winter or at night, the mixing is largely driven by the convection due to radiative heat loss to the atmosphere, whereas during the summer, the mixing is mainly shear-driven, since the wind

*Corresponding author
Email addresses: neeraja@bpi.cam.ac.uk (Neeraja Bhamidipati), sandre@mit.edu (Andre N. Souza), glenn@lake.mit.edu (Glenn R. Flierl)

stress at the surface is the primary mixing agent. Although the surface wind stress acts to stir light water downwards, most of this energy dissipates rapidly within the top $25-30$ m of the ocean. During the summer, increased solar heating of the surface water leads to more stable density stratification, reducing the penetration of wind-driven mixing. Wintertime cooling over the ocean always reduces stable stratification, allowing a deeper penetration of wind-driven turbulence but also generating plumes that can penetrate to great depths (Kraus and Turner, 1967). Therefore, regionally, the mixed layer can become much deeper when convective processes are active (Kara et al., 2003).

From a biological perspective, the ocean mixed layer is nutrient-poor, and its depth determines the average level of light seen by phytoplankton. Therefore, the mixing at the base of the ocean mixed layer is crucial for biological productivity. Since marine biological net primary production is the first step in the food chain of marine organisms, its decline could have severe consequences for fish stock and fisheries (Kuhlbrodt et al., 2009). Biological productivity is also important from a climate point of view: carbon fixation by phytoplankton constitutes a biological pathway for removing some of the anthropogenic CO_2 introduced into the atmosphere. Therefore primary production is also of considerable interest to oceanographers because it contributes significantly to global photosynthesis and ocean carbon uptake (Riebesell et al., 2007; Takahashi et al., 2009).

Proper parameterization of turbulent mixing in the ocean surface layer is crucial to simulate dynamics in the ocean interior, air–sea exchanges, and sea surface temperature correctly. If model parameterizations are to describe the upper ocean mixing processes accurately, they must be strongly physically based. The existing parameterizations of mixed layer dynamics range from the simple bulk mixed layer models (Kraus and Turner, 1967; Niiler and Kraus, 1977; Price et al., 1986) to models including non-local effects of mixing (Large et al., 1994). The bulk mixed layer model of Kraus–Turner uses an integrated form of the turbulent kinetic energy (TKE) equation, in which the balance is between the generation of turbulence by wind driven mixing and convection, with the work done in overturning the deep stable stratification (Kraus and Turner, 1967). Although such bulk models are popular, they might lose distinctive features such as the non-local transport because of the vertical integrals, and the assumption of homogenization may breakdown.

Other models require equations for turbulent kinetic energy and its rate of dissipation to estimate the vertical eddy diffusivity. These equations come from carrying out Reynolds decomposition on the Navier-Stokes equations, into a mean flow and a fluctuating component. Since these equations are no longer closed, closure assumptions are required (Acreman and Jeffery, 2007). Common to several of the first-order closure schemes is the assumption that the fluxes depend linearly on the property gradient, with an appropriate constant of proportionality, which is the eddy diffusivity. Other parameterizations have represented the eddy diffusivity as a function of the Richardson number (Pacanowski and Philander, 1981). Mellor and Yamada (1982) present a second-order turbulent closure model which solves equations for the turbulent kinetic energy and its

product with the turbulent length scale. This second-order closure comes from an assumption that the turbulent energy produced by shear and convection is balanced locally by turbulent dissipation. The K-Profile parameterization (KPP) scheme represents the turbulent mixing of buoyancy using a diffusion equation which has a vertically varying diffusivity along with a counter-gradient term which accounts for non-local transport, whereas the transport of passive tracers is still treated locally (Large et al., 1994). There have also been significant advancements towards enhancement of the KPP scheme, to include the effects of bottom boundary layer (Durski et al., 2004) and Langmuir turbulence (McWilliams and Sullivan, 2000; Smyth et al., 2002). Non-local effects have also been incorporated into schemes other than KPP such as the bulk mixed-layer models (Price et al., 1986), but these are generally ad-hoc.

Recent efforts to parameterize mixing in the ocean boundary layer include the works of Qiao et al. (2004), McWilliams et al. (2009), Li and Fox-Kemper (2017), Reichl and Hallberg (2018), and Reichl and Li (2019). On the other hand, some plume type atmospheric models include a non-local aspect for the transport of a passive tracer since the plumes transport the tracer from the level they start from (Romps and Kuang, 2011; Tan et al., 2018). The work on transilient theory (Stull, 1984; Stull and Kraus, 1987; Stull, 1993) is valuable in describing the theory and the merits of such an approach to model the non-local vertical transport by eddies in the upper ocean. The transilient matrix $\mathcal{K}$ describes the vertical transport by eddies, where each column corresponds to an initial height and each row corresponds to a final height: the element $\mathcal{K}_{ij}$ describes transport from z_j to z_i. If this matrix can be diagnosed for a convecting fluid, it can provide valuable information on the transilient (i.e., non-local) transport by eddies (Romps and Kuang, 2011).

We begin with a general statement of the relationship between the ensemble mean gradients $\mathcal{G}_i(x, y, z, t)$ and the ensemble mean fluxes $\mathcal{F}_i(x, y, z, t)$ of a scalar (where the subscript represents different components). The equation for the fluctuations (the deviations from the mean) is linear and is forced by the advection of the mean gradients by the fluctuating velocity; therefore the scalar fluctuations and the fluxes are linear functionals of the mean gradients:

$$\mathcal{F}_i(x, y, z, t) = -\int \mathcal{K}_{ij}(x, y, z, t|x', y', z', t')\mathcal{G}_j(x', y', z', t')\,\mathrm{d}x'\,\mathrm{d}y'\,\mathrm{d}z'\,\mathrm{d}t' \quad (1)$$

where the summation convention is used for repeated indices.

In this paper, we focus on estimating this exact formulation of the flux as a functional of the property gradient, using high resolution simulations to determine the form of the functional. For the mixed layer, we can reduce the order of the kernel by assuming that the statistics have no horizontal variation so that it becomes $\mathcal{K}(z, t|z', t')$. Finally, to further simplify the computation and the portrayal of the kernel, we will deal with the statistically steady state. This will be appropriate if the time-scales for the changes in the tracer distribution or the other mixed layer properties are slow enough. Furthermore, we use temporal and spatial averages instead of ensemble averages. In this idealized case, the

appropriate eddy diffusivity kernel $\mathcal{K}(z|z')$ describes the vertical transport by eddies at any vertical location z arising from gradients at z'. We emphasize that the work here does not propose a new parameterization; to do that, many of the effects such as winds and time-dependence would need to be brought back in and examined carefully. Instead, our study provides insight into how fluxes are related to gradients, gives an example of such a calculation, and, we hope, suggests approaches to parameterization.

For simplicity, we restrict our focus to convection-driven mixing using an idealized 2D surface layer of the ocean, where a balance of fluxes persists long enough for the system to reach a dynamical equilibrium. Although 3D effects appear soon after the onset of convective instability, the 2D problem can describe both the instability and some of the effects of non-linearity. For example, Taylor and Ferrari (2010) find good agreement of the mean profiles and turbulent features between 2D and 3D large eddy simulations of slantwise convection with a horizontal buoyancy gradient, forced by either surface wind stress or surface buoyancy flux. Furthermore, while 2D simulations do not work well for fingering convection in the limit of low Prandtl number Garaud and Brummell (2015), Schmalzl et al. (2004) find that, for higher values of the Prandtl number ($Pr > 1$), the flow structure and global quantities (e.g., Nusselt number and Reynolds number) exhibit similar behavior in 2D and 3D simulations. In the context of atmospheric boundary layer convection, Moeng et al. (2004) have found that certain properties, such as the vertical distribution of heat flux, are not sensitive to the choice of 2D versus 3D, although the same may not hold true when there is a mean shear. The authors argue that 2D models can be themselves thought of as a parameterization of 3D physics.

In §2, we discuss the basic equations governing the 2D system and derive an equation for the mixed layer depth (MLD), based on a balance between the imposed flux es. We also present the results from our 2D DNS to describe the evolution of buoyancy in the domain. In §3, we use passive tracers to describe the turbulent mixing in terms of an eddy diffusivity kernel, and propose a method to compute the kernel based on a proper representation of the physics. Although the analysis in this section corresponds to a 2D model of ocean turbulence, the framework described here applies equally well to a fully turbulent 3D case. Finally, in §4, we discuss the relevance of this study and indicate further directions for future work.

2. Governing equations

We begin with the two-dimensional Boussinesq equations.

$$\nabla \cdot \mathbf{u} = 0 \tag{2a}$$

$$\frac{\partial \mathbf{u}}{\partial t} + (\mathbf{u} \cdot \nabla)\mathbf{u} = -\frac{\nabla p}{\rho_o} + \nu \nabla^2 \mathbf{u} + b\hat{z} \tag{2b}$$

$$\frac{\partial b}{\partial t} + \mathbf{u} \cdot \nabla b = \kappa \nabla^2 b + \frac{\mathrm{d}}{\mathrm{d}z}(Q(z)) \tag{2c}$$

where $\mathbf{u} = (u, w)$ is the fluid velocity, p is the pressure, ρ_o is the mean density, ν is kinematic viscosity, and κ is thermal diffusivity. We assume that the fluid buoyancy b is a function only of temperature T, so that $b = \alpha g T$, where α is the coefficient of thermal expansion and g is acceleration due to gravity. The equation governing buoyancy has an added internal heating term to account for penetrative solar radiation. This flux is represented as $Q(z) = Q_o e^{z/l}$, where $Q_o = H_o(\alpha g)/(\rho_o C_p)$, H_o is the surface heat flux, C_p is the specific heat capacity of the fluid, l is the vertical decay scale, and z is the vertical space coordinate, negative downward with origin at sea level. The attenuation length l for solar radiation of short wavelength is approximately 20 m, whereas longer wavelengths get absorbed over a much shallower depth, approximately 0.5 m (Paulson and Simpson, 1977). Therefore, we use $l = 20$ m. In general, the surface heat flux varies both diurnally and seasonally, but here we restrict our attention to a constant surface heat flux to study the statistical steady state.

We assume that the top and bottom boundaries are free-slip and impermeable. The buoyancy flux at the bottom boundary is that necessary to maintain the Brunt–Väisälä frequency of the thermocline.

$$\left.\begin{aligned} w = 0, \quad \frac{\partial u}{\partial z} = 0, \quad \kappa \frac{\partial b}{\partial z} = \kappa N^2 \quad \text{at} \quad z = -H \\ w = 0, \quad \frac{\partial u}{\partial z} = 0 \qquad \text{at} \quad z = 0 \end{aligned}\right\} \tag{3}$$

with $H \gg l$. We further assume that a radiative cooling at the surface is specified so that the net flux in the system is zero, and the system reaches a statistical steady state. This simplification allows us to estimate a kernel that is stationary in time and only depends on the stationary statistics of the flow field. Furthermore, although we use this specific scenario in which a quasi-steady state approximation applies because of a net balance of fluxes, we emphasize again that subsequent approach to represent mixing in the surface layer as a functional of the mean gradients can be extended to a more general time-varying problem, where the eddy flux kernel is given as $\mathcal{K}(z, t|z', t')$ (cf. equation (1)).

Taking the horizontal average of equation (2c), where $\overline{*} = L^{-1}\int_0^L * \, \mathrm{d}x$ denotes horizontal average, we obtain the boundary condition for buoyancy at $z = 0$, i.e., the radiative cooling at the surface,

$$\frac{\partial \overline{b}}{\partial t} = -\frac{\partial}{\partial z}\left(\overline{w'b'} - Q_o e^{z/l} - \kappa \frac{\partial \overline{b}}{\partial z}\right) \tag{4}$$

where $b'(x, z, t)$ is the buoyancy perturbation ($b = \overline{b}(z, t) + b'(x, z, t)$). Assuming a quasi-steady evolution so that $\partial \overline{b}/\partial t = 0$, and integrating over the depth of the domain from $z = -H$ to $z = 0$ gives the boundary condition for buoyancy at $z = 0$,

$$\kappa \frac{\partial \overline{b}}{\partial z}\bigg|_{z=0} = \kappa N^2 - Q_o(1 - e^{-H/l}) \tag{5}$$

Table 1: Values of dimensionless parameters used in simulations, where h is the MLD.

L_x	L_z	Pr	F	Φ	(N_x, N_z)	$h = \ln \frac{F}{\Phi}$
4	16	10	8×10^6	8×10^5	(128,512)	2.302
4	16	10	1.6×10^7	8×10^5	(128,512)	2.996
4	16	10	2.4×10^7	8×10^5	(128,512)	3.401
4	16	10	3.2×10^7	8×10^5	(128,512)	3.689

The system is in dynamical equilibrium, and so we expect it to reach a statistical steady state. If $\partial b/\partial z < 0$ at the surface, we have colder fluid overlying hotter fluid. Therefore, $Q_o/\kappa N^2 > 1$ is a necessary condition for convection to occur, but it is not a sufficient condition since the fluid also needs to overcome viscous forces, as defined by the Rayleigh number. We non-dimensionalize the problem by defining the following dimensionless variables.[1]

$$\tilde{t} = \frac{t\kappa}{l^2}, \qquad \tilde{\mathbf{u}} = \frac{\mathbf{u}l}{\kappa}, \qquad \widetilde{b} = \frac{bl^3}{\kappa^2}, \qquad \tilde{p} = \frac{p\rho_o l^2}{\kappa^2} \tag{6}$$

The dimensionless equations are (dropping the tildes)

$$\nabla \cdot \mathbf{u} = 0 \tag{7a}$$

$$\frac{\partial \mathbf{u}}{\partial t} + (\mathbf{u} \cdot \nabla)\mathbf{u} = -\nabla p + \mathrm{Pr}\nabla^2 \mathbf{u} + b\hat{z} \tag{7b}$$

$$\frac{\partial b}{\partial t} + \mathbf{u} \cdot \nabla b = \nabla^2 b + Fe^z \tag{7c}$$

where the following non-dimensional parameters are defined

$$F = \mathrm{Pr}\ \mathrm{Ra}_f = \frac{Q_o l^4}{\kappa^3},\ \mathrm{Pr} = \frac{\nu}{\kappa},\ \mathrm{Ra}_f = \frac{Q_o l^4}{\nu\kappa^2},\ \Phi = \frac{N^2 l^4}{\kappa^2} \tag{8}$$

where Pr is the Prandtl number and Ra_f is the flux Rayleigh number. The dimensionless boundary conditions are now given by,

$$\left.\begin{aligned} w = 0, \quad \frac{\partial u}{\partial z} = 0, \quad \frac{\partial b}{\partial z} = \Phi \quad \text{at } z = -L_z \\ w = 0, \quad \frac{\partial u}{\partial z} = 0, \quad \frac{\partial b}{\partial z} = \Phi - F(1 - e^{-L_z}) \ \text{ at } z = 0 \end{aligned}\right\} \tag{9}$$

where $L_z = H/l$ is the dimensionless depth of the domain. The domain extends from 0 to L_x in the horizontal direction. We assume zero base flow so that the fluid velocity is given by the perturbation velocity $\mathbf{u}'$ ($\mathbf{u} = \mathbf{0} + \mathbf{u}'$, where $\mathbf{u}' = (u', w')$).

[1] Note that our particular choice of non-dimensionalization is arbitrary since we do not make any approximations on the basis of the non-dimensionalization.

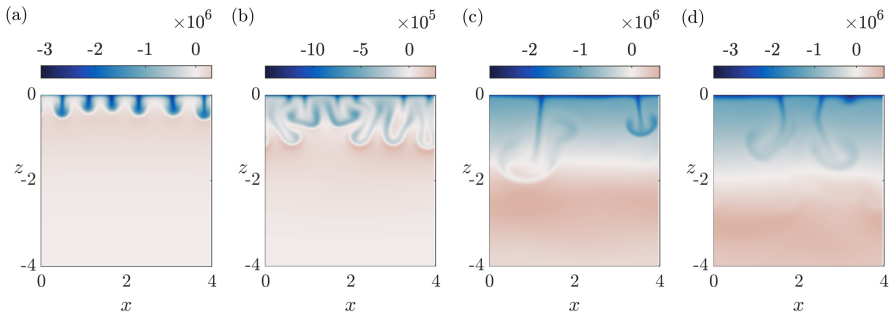

Figure 1: (Color figure) The panels show the evolution of the deviation of buoyancy field, $b(x, z, t) - \Phi z$, at four times, $t = 0.03, 0.04, 0.49, 1.10$ for $F/\Phi = 20$.

We solve equations (7a–c) using the Dedalus pseudo-spectral code (Burns et al., 2019). We discretize the domain using N_x Fourier modes in the horizontal direction and N_z Chebyshev modes in the vertical direction, so that the smallest length scales in the vertical are $\mathcal{O}(10)$ mm and the resolution at the base of the mixed layer is $\mathcal{O}(100)$ cm for our chosen parameter values. For time-stepping, we use a two-stage second-order Runge-Kutta method, where the linear terms are treated implicitly, and non-linear terms are treated explicitly. The time-step size is set by a Courant-Friedrichs-Lewy condition with prefactor 0.5. We choose a sufficiently large domain depth in order to mitigate the effects of internal gravity waves, generated by turbulent plumes hitting the base of the mixed layer, reflecting off of the bottom boundary. Table 1 shows the range of parameter values used in the simulations.

We initialize the problem by specifying a linear buoyancy field $b = \Phi z$, and adding a small perturbation. Because of the surface cooling, the perturbation to buoyancy field produces horizontal buoyancy gradients which, in turn, begin to produce vorticity. The flows will further lift the light fluid and draw the heavier fluid down; the layer tries to overturn. Figure 1 shows the evolution of the deviation of buoyancy field, $b - \Phi z$, in the domain. In figure 1(a)-(d), the four panels show convective plumes descending from the surface, and generating dipolar vortices which increase the downward speed. Note the internal waves, generated as the plume hits the stratified base of the convective region. The plumes drive the turbulent mixing of the linear buoyancy field forming a fairly homogeneous region – a mixed layer – which deepens over time. Figure 2(a) shows the time-evolution of the horizontally averaged buoyancy field $\overline{b}$ in the domain, starting with an initially linear profile. The depth of this mixed region initially grows as $\sqrt{t}$ as expected of penetrative convection (Van Roekel et al., 2018), but eventually settles to a constant value (figure 2(b)).

We can estimate the MLD, h, using convective adjustment ideas; however, the naive approach of adjusting the diffusive profile that matches the boundary condition ends up with non-zero heat flux divergence. Instead, we can solve the initial value problem starting with the constant stratification and turning on

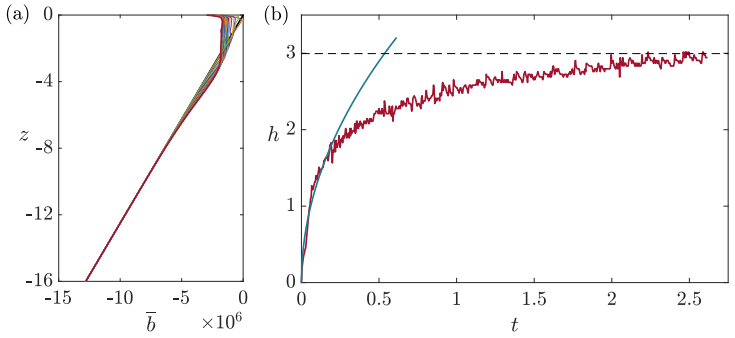

Figure 2: (Color figure) (a) Horizontally averaged buoyancy $\overline{b}$ plotted at various times as represented by the different colors, starting with a linear profile (black line) at $t = 0$. (b) The variation of MLD h versus time t. The horizontal line represents $h = \ln(F/\Phi)$ and the blue curve represents $h \sim \sqrt{t}$. Here, the ratio of the penetrating shortwave heat flux to the diffusive heat flux in the deep thermocline is $F/\Phi = 20$.

the radiative heat flux in the interior and boundary conditions, with convective adjustment occurring whenever $\partial\overline{b}/\partial z < 0$. However, the end state can be found by setting $\partial\overline{b}/\partial t = 0$ in the non-dimensional form of equation (4) and integrating up from the bottom to find

$$\overline{w'b'} - Fe^z - \frac{\partial \overline{b}}{\partial z} = -\Phi \tag{10}$$

(neglecting the radiative flux at the bottom of the domain, i.e., $e^{-H/l} \approx 0$ for $H \gg l$). When $Fe^{-h} = \Phi$, the flux balance in the water below the mixed layer will be achieved for $\partial\overline{b}/\partial z = 0$ at $z = -h$. In the convecting layer, we must also have $\overline{w'b'} - \partial\overline{b}/\partial z = 0$ at that depth. This is consistent with the mixed layer buoyancy being constant and the eddy flux vanishing at the base of the mixed layer. Thus we settle to a constant flux state when

$$h = \ln\left(\frac{F}{\Phi}\right) \tag{11}$$

so that the mixed layer descends to the depth where the gradient of $\overline{b}$ in the diffusive solution changes sign.[2] Overshooting plumes may lead to some mixing below this depth resulting in a reversal in sign of the buoyancy flux; however, that is weak in the experiments since the mixed layer depth is comparable to the attenuation length for solar radiation. Choosing the base of the mixed layer to be where $\overline{w'b'} = 0$ still gives the value given by equation (11) since the gradient of $\overline{b}$ is nearly zero at $z = -h$ (see figure 2(a)). Near the surface, the eddy flux

[2]From equation (4), the deepening effectively halts and we reach a steady state when the buoyancy flux from the convective plumes can balance the heat fluxes.

$\overline{w'b'}$ vanishes so that the balance is between the diffusive flux and the solar heating. Correspondingly, the horizontally averaged buoyancy profile shows a negative gradient close to the surface. In contrast, within the mixed layer, the vertical convective flux nearly balances the heating throughout the mixed layer.

Henceforth, we describe the mixed layer depth (MLD) using the non-dimensional parameter, F/Φ, which is the ratio of the penetrating heat flux to the diffusive heat flux in the deep thermocline (see table 1).

3. The eddy diffusivity kernel

3.1. Mixing of a passive scalar

Equation (7c) is analogous to an advection–diffusion equation for a passive scalar given by

$$\frac{\partial c}{\partial t} + \mathbf{u} \cdot \nabla c = \nabla^2 c + \frac{\mathrm{d}}{\mathrm{d}z}(f(z)) \tag{12}$$

where $c(x, z, t)$ is the concentration of tracer, and $f(z)$ is a forcing function or source term for the tracer. Additionally, we define the boundary conditions for the tracer,

$$\frac{\partial c}{\partial z} = 0 \qquad \text{at} \quad z = 0, -L_z \tag{13}$$

Taking a horizontal average of equation (12) and using the continuity equation,

$$\frac{\partial \overline{c}}{\partial t} + \frac{\partial}{\partial z}\overline{w'c'} = \frac{\partial^2 \overline{c}}{\partial z^2} + \frac{\mathrm{d}}{\mathrm{d}z}(f(z)) \tag{14}$$

Splitting the concentration into a horizontally averaged part and a fluctuating part ($c = \overline{c}(z, t) + c'(x, z, t)$) and substituting this into equation (12) we obtain (after subtraction of equation (14))

$$\left(\frac{\partial}{\partial t} + \mathbf{u}.\nabla - \nabla^2\right)c' - \frac{\partial}{\partial z}\overline{w'c'} = -w'\frac{\partial \overline{c}}{\partial z} \tag{15}$$

The integro-differential operator on the left-hand side is linear if we have a specified flow field $\mathbf{u}$, so we can easily show that c' and the eddy flux $\overline{w'c'}$ will be a linear functionals of $\partial\overline{c}/\partial z$. This implies that the horizontally and temporally averaged fluxes are a functional of the horizontally and temporally averaged gradients,

$$\langle w'c' \rangle = -\int \mathcal{K}(z|z')\frac{\partial \langle c \rangle (z')}{\partial z'}\mathrm{d}z' \tag{16}$$

with $\langle * \rangle = \lim_{\tau\to\infty} \tau^{-1} \int_0^\tau \overline{*}\, \mathrm{d}t$ (see appendix A).

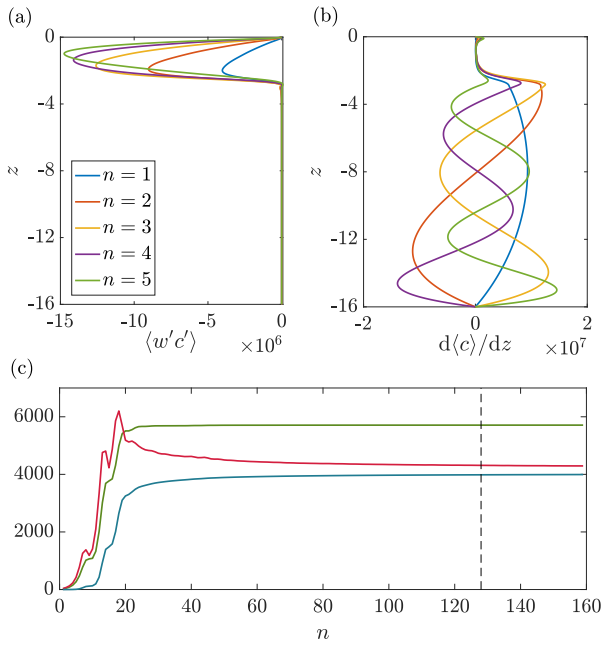

Figure 3: (Color figure) (a) and (b) show the horizontally averaged eddy fluxes and gradients of tracer concentration corresponding to $f_n(z)$ where $n = 1, 2, 3, 4, 5$. (c) Convergence of the kernel $\mathcal{K}(z|z')$ with n in terms of the maximum eigenvalue (multiplied by 100 for scale, green curve), sum of the absolute values of $\mathcal{K}(z|z')$ (red curve), and the sum of the squares of $\mathcal{K}(z|z')$ (blue curve). The vertical line represents $n = 128$. Here, the ratio of the penetrating shortwave heat flux to the diffusive heat flux in the deep thermocline is $F/\Phi = 10$.

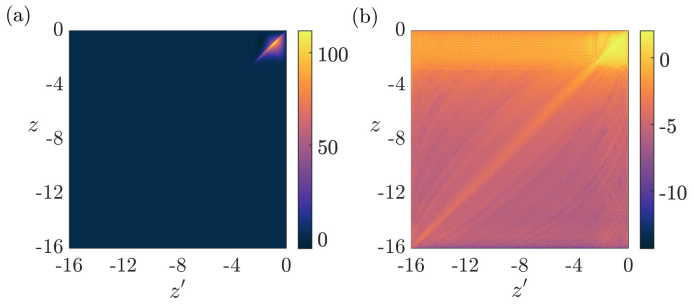

Figure 4: (Color figure) (a) $\mathcal{K}(z|z')$. (b) $\log_{10}|\mathcal{K}(z|z')|$. Here, the ratio of the penetrating shortwave heat flux to the diffusive heat flux in the deep thermocline is $F/\Phi = 10$, and the kernel is computed using $n = 128$ tracers.

In the discrete form used for the numerics, equation (16) can be written for a particular forcing function f_k as

$$\langle w'c'\rangle_{ik} = -\mathcal{K}(z_i|z_j)\frac{\partial\langle c\rangle_j}{\partial z'_k}\Delta z_j = -\mathcal{K}_{ij}\frac{\partial\langle c\rangle_j}{\partial z'_k}\Delta z_j \tag{17}$$

with the appropriate summation convention; the goal is to find the matrix $\mathcal{K}_{ij}$. We solve equation (12) from zero initial conditions, holding $f = f_1(z)$ fixed, and compute to a statistical steady state giving one pair of $\langle w'c'\rangle_{i,1}$ and $\langle c_z\rangle_{i,1}$ vectors. We repeat the experiment n times, using n passive tracers to reach n linearly independent statistically steady states (see appendix B).

Collecting the experiments into $m \times n$ matrices, with $m = 512$ being the number of modes used to discretize the domain in z and n being the number of tracers, gives $\mathcal{F} \equiv \langle w'c'\rangle_{ik}$ and $\mathcal{G} \equiv \Delta z_j\big(\partial\langle c\rangle_j/\partial z_k\big)$. The eddy diffusivity kernel $\mathcal{K}$ can be estimated using a least-squares fit of the discrete data as $\mathcal{K} = -\mathcal{F}(\mathcal{G}^T\mathcal{G})^{-1}\mathcal{G}^T$.

Figures 3(a),(b) show the fluxes and gradients of the passive scalar for $n = 1, 2, 3, 4, 5$. Figure 3(c) shows the convergence of the kernel with n as we add more tracers to compute the fluxes and gradients. We choose $n = 128$ tracers since the results do not vary significantly as we add more tracers (figure 3(c)).

Figure 4(a) shows the kernel for $n = 128$ tracers and for a given ratio of the penetrating shortwave heat flux to the diffusive heat flux in the deep thermocline ($F/\Phi = 10$).. In this figure, the horizontal axis gives the center of a delta function forcing for an arbitrary function $f(z)$ represented as the sum of delta functions, and the vertical axis gives the response, with the diagonal elements (going from lower-left to upper-right) representing the local contributions. Figure 4(a) illustrates that the mixing is strongest within the mixed layer, and the large off-diagonal elements illustrate that both local and non-local effects of mixing are significant within the convective region. Figure 4(b) shows the very weak eddy flux associated with the internal gravity waves in the region below the mixed layer.

Figure 5 shows the kernel for four different values of the mixed layer depth

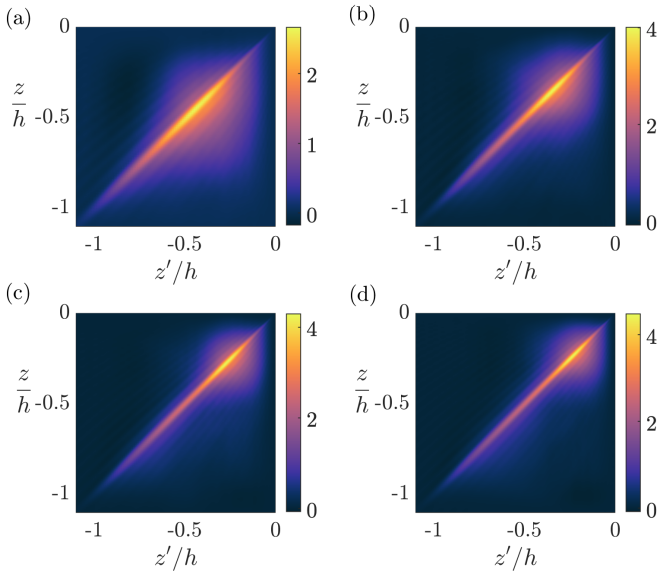

Figure 5: (Color figure) (a)-(d) show the kernel $\mathcal{K}(z/h|z'/h)$ for four different values of MLD, $h = \ln(F/\Phi)$, obtained by varying the ratio of the penetrating shortwave heat flux to the diffusive heat flux in the deep thermocline, where $F/\Phi = 10, 20, 30, 40$ respectively.

obtained by varying the non-dimensional parameter F/Φ. The local effects of mixing can be seen from the diagonal elements of $\mathcal{K}(z|z')$; this is shown in figure 6(a) where the vertical axis has been non-dimensionalized by MLD, $h = \ln(F/\Phi)$. The figure illustrates that the eddy diffusivity decays rapidly in the region outside the mixed layer, for $|z/h| > 1$. The non-local effects of mixing can be interpreted by looking at a horizontal slice in figure 5; this is shown in figure 6(b) for a location in the middle of the mixed layer. The figure shows the contributions from forcing at different levels to the response in eddy flux at $z/h = -0.5$, i.e., in the middle of the convecting layer. The figure illustrates that although the local effects are strongest as indicated by the peak at $z/h \approx -0.5$ i.e., that the flux at that level has the biggest contributions from the gradient at that level, more importantly, it highlights that the flux at that level also has leading-order contributions from gradients above that level. The stronger contributions from gradients above the forcing location are due to the convective plumes descending from the surface which have large momentum. However, we observe weak contributions from the gradients below this point due to the upward plumes having petered out by the time they reach the top.

3.2. Eddy flux of buoyancy

The analysis presented in §3.1 is strictly only applicable for a passive scalar since the fluxes $\langle w'c' \rangle$ are linear in c', whereas $\langle w'b' \rangle$ is non-linear since w' is a function of the buoyancy b. However, we can compare the eddy flux $\langle w'b' \rangle$

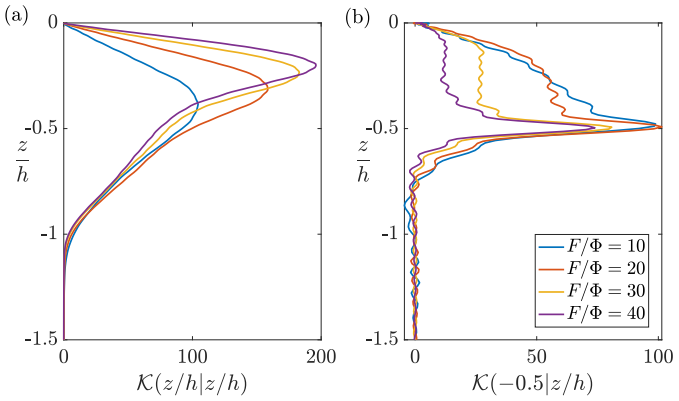

Figure 6: (Color figure) (a) The diagonal elements of the kernel, showing the local effect of the mixing, plotted against z/h, where h is the MLD, and (b) a horizontal slice of $\mathcal{K}(z/h|z'/h)$ in the middle of the mixed layer at $z/h = -0.5$ illustrating the non-local effects of mixing for four different values of MLD. In each case, the MLD is defined as the ratio of the penetrating shortwave heat flux to the diffusive heat flux in the deep thermocline, $h = \ln(F/\Phi)$.

obtained from the experiments to an estimate using the kernel $\mathcal{K}(z|z')$ and the diagnosed gradients $\partial\langle b\rangle/\partial z$. A comparison between the two fluxes is shown in figure 7(a) for four values of MLD.

It is worth noting that the flow is generated by the buoyancy b and that the kernel $\mathcal{K}$ is dependent on statistics of the flow field. While figure 7(a) illustrates that the estimate of the eddy flux using the kernel gives a consistent representation of the buoyancy fluxes, the same would not hold true if a buoyancy anomaly was created by a different active scalar affecting the flow field since this is not taken into account in estimating $\mathcal{K}$. Nevertheless, this calculation does indeed show that the kernel is in fact consistent with the fluxes of buoyancy. Additionally, it is also worth noting that although the fluxes do decay rapidly outside the convective region, for $|z/h| > 1$, the fluxes are non-linear and we do not expect a self-similar solution applicable to all examples of convective mixing. Indeed, we see that the kernel is not similar in z/h even for a passive scalar (figure 6).

We further investigate the importance of non-local effects by defining an effective local diffusivity $\mathcal{D}(z)$,

$$\mathcal{K}(z|z') = \mathcal{D}(z)\delta(z - z') \implies \mathcal{D}(z) = \int \mathcal{K}(z|z')dz' \tag{18}$$

The estimates of the flux using the appropriate local diffusivity is shown in figure 7(b), which illustrates the significance of the non-local terms in describing the transport both qualitatively and quantitatively.

4. Conclusions and future work

The mixing of a passive tracer in the the surface mixed layer of the ocean is given by a non-local formulation of the eddy flux in terms of the mean gradient,

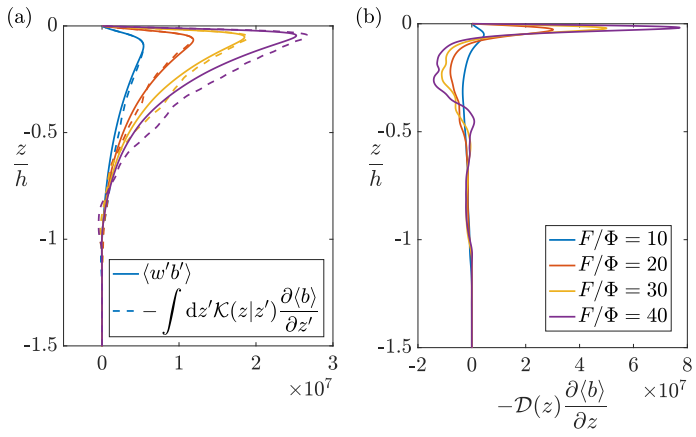

Figure 7: (Color figure) (a) Comparison of the eddy fluxes $\langle w'b' \rangle$ (solid curve) with the estimate from the kernel $-\int \mathrm{d}z' \mathcal{K}(z|z') \partial b/\partial z$ (dashed curve) for four different MLD. (b) An estimate of the flux using the appropriate local diffusivity $\mathcal{D}(z)$ four different values of MLD. In each case, the MLD is defined as the ratio of the penetrating shortwave heat flux to the diffusive heat flux in the deep thermocline, $h = \ln(F/\Phi)$.

$\langle w'c' \rangle = -\int \mathrm{d}z' \mathcal{K}(z|z') \partial \langle c \rangle / \partial z'$, where $\mathcal{K}(z|z')$ is the eddy diffusivity kernel. Although several non-local parameterizations have been defined in literature, the analysis presented in this paper does not use any closure assumptions, and therefore the functional form of eddy diffusivity gives an unapproximated representation of the chosen physics. We demonstrate that the eddy flux can be expressed as a functional of the gradient, and compute the full eddy diffusivity kernel by resolving the small scales.

We consider an idealized 2D convection-driven mixed layer dynamics and give an estimate for MLD as given by a balance between the surface fluxes and the buoyancy flux of the thermocline; this analysis is therefore directly applicable to situations where convection is the dominant process in causing mixed layer deepening. To further illustrate that this analysis is equally applicable to a 3D case, we have looked at an example of the balanced state in three dimensions and find that the structure of the gradients and fluxes of both buoyancy and passive tracer are very similar to the 2D DNS (see figure 8).

The mixed layer deepens as the surface fluxes are increased relative to the buoyancy fluxes at the thermocline, in accordance with the theoretical formulation of MLD. At early times, the mixed layer deepens as square root of time, but eventually settles to a near constant value given by the location where the fluxes due to solar heating balance the buoyancy flux of the thermocline.

The kernel describes both the local and non-local effects of mixing, illustrating that for this flow, the non-local effects are strongest closer to the surface because of the energy of the convective plumes detaching from the surface. The non-local effects are therefore important in transporting properties from one side of the boundary layer to the other as illustrated in figure 1. To further un-

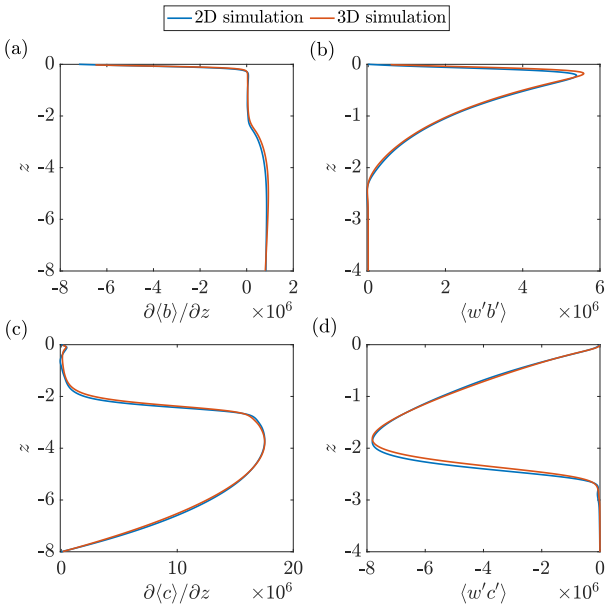

Figure 8: (Color figure) Comparison of the horizontally and temporally averaged fluxes and gradients of buoyancy and passive tracer in 2D and 3D simulations with the same boundary conditions. The 3D simulations are done using a finite volume code (Ramadhan et al., 2020) whereas the 2D simulations use a pseudo-spectral code (Burns et al., 2019). In both sets of simulations, the ratio of the penetrating shortwave heat flux to the diffusive heat flux in the deep thermocline is $F/\Phi = 10$, so that the MLD is $h = \ln(F/\Phi) \approx 2.3$. The profiles for the passive tracer are estimated by solving equation (12) where $f(z)$ is given by equation (B.2) for $n = 1$.

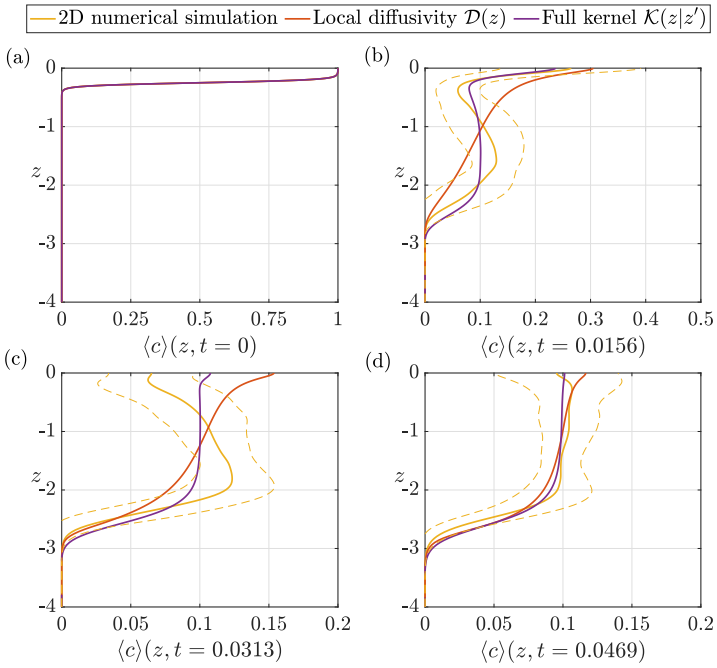

Figure 9: (Color figure) The time-evolution of a passive tracer added to the flow near the surface, as given by the 2D DNS, and solution to equations (19a) and (19b). The yellow dotted curves represent 1 standard deviation from the mean ensemble profile (yellow curve) obtained by averaging 100 realizations in the 2D DNS. (a) shows the initial profile at $t = 0$ which is given by equation (20) for $d = 0.25$. The ratio of the penetrating shortwave heat flux to the diffusive heat flux in the deep thermocline is $F/\Phi = 10$.

derstand the mixing of a passive tracer by the flow, the importance of non-local effects can be illustrated by adding a tracer near the surface and studying its distribution a short time later. To do this, we solve

$$\frac{\partial \langle c \rangle}{\partial t} = \frac{\partial}{\partial z}\left(\mathcal{D}(z)\frac{\partial \langle c \rangle}{\partial z}\right) + \frac{\partial^2 \langle c \rangle}{\partial z^2} \tag{19a}$$

$$\frac{\partial \langle c \rangle}{\partial t} = \frac{\partial}{\partial z}\left(\int \mathcal{K}(z|z')\frac{\partial \langle c \rangle}{\partial z'}\mathrm{d}z'\right) + \frac{\partial^2 \langle c \rangle}{\partial z^2} \tag{19b}$$

which describe the time-evolution of the ensemble-averaged concentration $\langle c \rangle(z,t)$ as mixed by the diagnosed local diffusivity $\mathcal{D}(z)$ given by equation (18) and the full kernel $\mathcal{K}(z|z')$ respectively. Since the flow is in a statistically steady state, we would expect that the tracer distribution given by the solution to both equations (19a) and (19b) would be very similar at late times. We begin with

$$\langle c \rangle(z, t=0) = \frac{1}{2}\big[\tanh(20(z+d)) + 1\big] \tag{20}$$

The equivalent profiles from the 2D DNS can be obtained by adding passive tracers to the statistically steady flow, i.e., solving equation (12) with $f(z) = 0$, and with the same initial condition for the tracer concentration $c(x, z, t)$ (equation (20)). We add 100 tracers to the flow at different times to obtain the ensemble and horizontally averaged profiles $\langle c \rangle(z,t)$. This is shown in figure 9. As the figure illustrates, the profiles given by the full kernel better describe the transient evolution of the tracer at early times. The profiles obtained using (equation (19b)) are within 1 standard deviation of the profiles obtained from the 2D DNS, whereas the equivalent profiles from the local diffusivity (equation (19a)) lie outside this range. Although both solutions (equations (19a) and (19b)) converge rapidly, the figure highlights that the kernel contains information pertaining to the non-locality of the flow that is missing from a local diffusivity. This non-local behavior might be especially important for transient processes that occur on short timescales, where the non-local fluxes could lead to qualitative macroscopic differences in properties in the ocean mixed layer.

The kernel $\mathcal{K}(z|z')$ depends on the statistics of the flow field and is computed here for advection of a passive scalar by a fully non-linear turbulent flow field. Within the mixed layer, the kernel is non-local since plumes transport properties from one level to the other by advection. The non-local fluxes move the tracer around with an advective timescale, whereas a purely diffusive description could exhibit a different timescale dependence on mixed layer depth. This non-locality could be particularly important when the mixed layer is very deep since stronger convective plumes will tend to transport properties over larger distances by advection.

One further development would be to study seasonal variations of MLD by adding a time-varying surface insolation to see if the quasi-steady approach is adequate in describing time-varying fluxes. Although our model is missing important processes for the surface layer of the ocean (e.g. winds), we have

established a framework for parameterizing fluxes using a functional form of eddy diffusivity which is based on proper representation of the physics for different flow problems. While the particular example presented here is limited, it illustrates the basic principle of using a functional approach and points to a way to define those functionals for other problems in turbulence concerning the mixing of a passive scalar.

Appendix A

Let ϕ' be the Green's function for the integro-differential operator on the left hand side of equation (15), so that

$$\left(\frac{\partial}{\partial t} + \mathbf{u}.\nabla - \nabla^2\right)\phi'(\mathbf{x}, t|\mathbf{x}', t') - \frac{\partial}{\partial z}\overline{w'\phi'} = \delta(\mathbf{x} - \mathbf{x}')\delta(t - t') \tag{A.1}$$

Multiplying equation (A.1) by $-w'(\mathbf{x}', t')\partial\overline{c}(z', t')/\partial z'$ and integrating with respect to $\mathbf{x}'$ and t' shows by comparison with equation (15) that

$$c'(\mathbf{x}, t) = -\int \mathrm{d}\mathbf{x}'\ \mathrm{d}t'\ \phi'(\mathbf{x}, t|\mathbf{x}', t')w'(\mathbf{x}', t')\frac{\partial\overline{c}(z', t')}{\partial z'} \tag{A.2}$$

Multiplying equation (A.2) by w' and taking a horizontal average gives the flux $\overline{w'c'}$ which is a function of z and t,

$$\overline{w'c'} = -\int \mathrm{d}z'\ \mathrm{d}t'\left[\int \mathrm{d}x'\ \overline{w'(\mathbf{x}, t)\phi'(\mathbf{x}, t|\mathbf{x}', t')w'(\mathbf{x}', t')}\right]\frac{\partial\overline{c}(z', t')}{\partial z'} \tag{A.3}$$

The term in square brackets is a kernel $\tilde{\mathcal{K}}(z, t|z', t')$ for the temporally evolving, horizontally averaged flux. Since $f(z)$ does not depend on time and the flow is in a statistically steady state, $\partial\overline{c}/\partial t$ is negligible. Therefore, the temporally and horizontally averaged flux becomes

$$\langle w'c'\rangle = -\int \mathrm{d}z'\left[\int \mathrm{d}x'\ \mathrm{d}t'\ \langle w'(\mathbf{x}, t)\phi'(\mathbf{x}, t|\mathbf{x}', t')w'(\mathbf{x}, t)\rangle\right]\frac{\partial\langle c\rangle(z')}{\partial z'} \tag{A.4}$$

with $\langle * \rangle = \lim_{\tau\to\infty} \tau^{-1}\int_0^\tau * \,\mathrm{d}t$. The kernel $\mathcal{K}(z|z')$ which maps the gradients to the fluxes is the term in the square brackets in equation (A.4).

$$\langle w'c'\rangle = -\int \mathcal{K}(z|z')\frac{\partial\langle c\rangle(z')}{\partial z'}\,\mathrm{d}z' \tag{A.5}$$

Ensemble (rather than spatial-temporal) averaging would lead to the same form after invoking stationarity and horizontal homogeneity, appropriate to our periodic domain.

Appendix B

To obtain linearly independent data pairs for both $\langle w'c' \rangle$ and $\partial \langle c \rangle / \partial z$, we could define the forcing function $f(z)$ as

$$f(z) \equiv f_k(z) = F \times \left(T_{k+1}\left(\frac{2z}{L_z} + 1\right) - \left(\frac{z}{L_z}\right)\left[T_{k+1}(1) - T_{k+1}(-1)\right] \right) \quad \text{(B.1)}$$

where $T_k(z) = \cos(k \cos^{-1}(z))$ are Chebyshev polynomials of first kind. This definition of $f_k(z)$, which includes the subtraction of a linear term, ensures that the domain averaged concentration, found by integrating equation (14) in z, remains constant in time and the system reaches a statistical steady state.

If we define $\mathrm{d}f(z)/\mathrm{d}z$ in a way that its vertical integral is not zero, i.e., without subtracting the linear part from $f(z)$, then we would have $\partial \overline{c}/\partial t$ tending to a constant. This, however, would no effect on the fluxes and gradients of tracer, and they would still converge to statistically steady values in time. Therefore in our simulations we have defined $f(z)$ as

$$f(z) \equiv f_n(z) = F \times \left[T_{n+1}\left(\frac{2z}{L_z} + 1\right) \right] \quad \text{(B.2)}$$

in order to estimate the kernel $\mathcal{K}(z|z')$ given by equation (16).

Acknowledgments

We thank the two anonymous reviewers for their critical feedback and suggestions on this manuscript. This work was conducted partly at the Geophysical Fluid Dynamics Program, Woods Hole Oceanographic Institution. The Geophysical Fluid Dynamics Program is supported by the National Science Foundation and the Office of Naval Research. GRF is also partly supported through a grant from the National Science Foundation (OCE-1459702).

References

Acreman, D.M., Jeffery, C.D., 2007. The use of Argo for validation and tuning of mixed layer models. Ocean Model. 19, 53–69. doi:10.1016/j.ocemod.2007.06.005.

Burns, K.J., Vasil, G.M., Oishi, J.S., Lecoanet, D., Brown, B.P., 2019. Dedalus: A Flexible Framework for Numerical Simulations with Spectral Methods. arXiv e-prints , arXiv:1905.10388arXiv:1905.10388.

Durski, S.M., Glenn, S.M., Haidvogel, D.B., 2004. Vertical mixing schemes in the coastal ocean: Comparison of the level 2.5 Mellor-Yamada scheme with an enhanced version of the K profile parameterization. J. Geophys. Res.: Oceans 109.

Garaud, P., Brummell, N., 2015. 2D or not 2D: the effect of dimensionality on the dynamics of fingering convection at low Prandtl number. Astrophys. J. 815, 42.

Kantha, L.H., Clayson, C.A., 1994. An improved mixed layer model for geophysical applications. J. Geophys. Res.: Oceans 99, 25235–25266. doi:10.1029/94jc02257.

Kara, A.B., Rochford, P.A., Hurlburt, H.E., 2003. Mixed layer depth variability over the global ocean. J. Geophys. Res.: Oceans 108.

Kraus, E.B., Turner, J.S., 1967. A one-dimensional model of the seasonal thermocline II. The general theory and its consequences. Tellus 19, 98–106. doi:10.3402/tellusa.v19i1.9753.

Kuhlbrodt, T., Rahmstorf, S., Zickfeld, K., Vikebø, F.B., Sundby, S., Hofmann, M., Link, P.M., Bondeau, A., Cramer, W., Jaeger, C., 2009. An integrated assessment of changes in the thermohaline circulation. Clim. Change 96, 489–537. doi:10.1007/s10584-009-9561-y.

Large, W.G., McWilliams, J.C., Doney, S.C., 1994. Oceanic vertical mixing: A review and a model with a nonlocal boundary layer parameterization. Rev. Geophys. 32, 363–403. doi:10.1029/94rg01872.

Li, Q., Fox-Kemper, B., 2017. Assessing the effects of Langmuir turbulence on the entrainment buoyancy flux in the ocean surface boundary layer. J. Phys. Oceanogr. 47, 2863–2886.

McWilliams, J.C., Huckle, E., Shchepetkin, A.F., 2009. Buoyancy effects in a stratified Ekman layer. J. Phys. Oceanogr. 39, 2581–2599.

McWilliams, J.C., Sullivan, P.P., 2000. Vertical mixing by Langmuir circulations. Spill Sci. Technol. Bull. 6, 225–237.

Mellor, G.L., Yamada, T., 1982. Development of a turbulence closure model for geophysical fluid problems. Rev. Geophys. 20, 851–875. doi:10.1029/rg020i004p00851.

Moeng, C.H., McWilliams, J.C., Rotunno, R., Sullivan, P.P., Weil, J., 2004. Investigating 2D modeling of atmospheric convection in the PBL. J. Atmos. Sci. 61, 889–903.

Niiler, P.P., Kraus, E.B., 1977. One-dimensional models of the upper ocean. Modelling Predict. Up. Layers Ocean , 143–172.

Pacanowski, R.C., Philander, S.G.H., 1981. Parameterization of vertical mixing in numerical models of tropical oceans. J. Phys. Oceanogr. 11, 1443–1451. doi:10.1175/1520-0485(1981)011<1443:POVMIN>2.0.CO;2.

Paulson, C.A., Simpson, J.J., 1977. Irradiance measurements in the upper ocean. J. Phys. Oceanogr. 7, 952–956. doi:10.1175/1520-0485(1977)007<0952:imituo>2.0.co;2.

Price, J.F., Weller, R.A., Pinkel, R., 1986. Diurnal cycling: Observations and models of the upper ocean response to diurnal heating, cooling, and wind mixing. J. Geophys. Res.: Oceans 91, 8411–8427. doi:10.1029/jc091ic07p08411.

Qiao, F., Yuan, Y., Yang, Y., Zheng, Q., Xia, C., Ma, J., 2004. Wave-induced mixing in the upper ocean: Distribution and application to a global ocean circulation model. Geophys. Res. Lett. 31.

Ramadhan, A., Wagner, G.L., Hill, C., Campin, J.M., Churavy, V., Besard, T., Souza, A., Edelman, A., Marshall, J., Ferrari, R., 2020. Oceananigans.jl: Fast and friendly geophysical fluid dynamics on GPUs. J. Open Source Softw. 4, 2018. doi:10.21105/joss.02018.

Reichl, B.G., Hallberg, R., 2018. A simplified energetics based planetary boundary layer (ePBL) approach for ocean climate simulations. Ocean Model. 132, 112–129.

Reichl, B.G., Li, Q., 2019. A parameterization with a constrained potential energy conversion rate of vertical mixing due to Langmuir turbulence. J. Phys. Oceanogr. 49, 2935–2959.

Riebesell, U., Schulz, K.G., Bellerby, R., Botros, M., Fritsche, P., Meyerhöfer, M., Neill, C., Nondal, G., Oschlies, A., Wohlers, J., et al., 2007. Enhanced biological carbon consumption in a high CO2 ocean. Nature 450, 545–548. doi:10.1038/nature06267.

Romps, D.M., Kuang, Z., 2011. A transilient matrix for moist convection. J. Atmos. Sci. 68, 2009–2025. doi:10.1175/2011jas3712.1.

Schmalzl, J., Breuer, M., Hansen, U., 2004. On the validity of two-dimensional numerical approaches to time-dependent thermal convection. Europhys. Lett. 67, 390.

Smyth, W.D., Skyllingstad, E.D., Crawford, G.B., Wijesekera, H., 2002. Nonlocal fluxes and Stokes drift effects in the K-profile parameterization. Ocean Dyn. 52, 104–115.

Stull, R.B., 1984. Transilient turbulence theory. part I: The concept of eddy-mixing across finite distances. J. Atmos. Sci. 41, 3351–3367.

Stull, R.B., 1993. Review of non-local mixing in turbulent atmospheres: Transilient turbulence theory. Bound.-Lay. Meteorol. 62, 21–96.

Stull, R.B., Kraus, E.B., 1987. The transilient model of the upper ocean. J. Geophys. Res.: Oceans 92, 10745–10755.

Takahashi, T., Sutherland, S.C., Wanninkhof, R., Sweeney, C., Feely, R.A., Chipman, D.W., Hales, B., Friederich, G., Chavez, F., Sabine, C., et al., 2009. Climatological mean and decadal change in surface ocean pCO2, and net sea–air CO2 flux over the global oceans. Deep Sea Res. II 56, 554–577. doi:10.1016/j.dsr2.2008.12.009.

Tan, Z., Kaul, C.M., Pressel, K.G., Cohen, Y., Schneider, T., Teixeira, J., 2018. An extended eddy-diffusivity mass-flux scheme for unified representation of subgrid-scale turbulence and convection. J. Adv. Model. Earth Syst. 10, 770–800. doi:10.1002/2017ms001162.

Taylor, J.R., Ferrari, R., 2010. Buoyancy and wind-driven convection at mixed layer density fronts. J. Phys. Oceanogr. 40, 1222–1242.

Van Roekel, L., Adcroft, A.J., Danabasoglu, G., Griffies, S.M., Kauffman, B., Large, W., Levy, M., Reichl, B.G., Ringler, T., Schmidt, M., 2018. The KPP boundary layer scheme for the ocean: Revisiting its formulation and benchmarking one-dimensional simulations relative to LES. J. Adv. Modelling Earth Syst. 10, 2647–2685.